Analysis of the CANDU 9 Shield Cooling in the Event of Loss of Forced Circulation Using the CATHENA Thermalhydraulic Code

N.K. Popov[1], L.A. Morris[2], D.N. Padhi[3]
Atomic Energy of Canada Limited
Sheridan Park, Mississauga, Ontario

ABSTRACT

The CANDU 9 shield cooling system is designed to facilitate enhanced thermosyphoning of the end shield inventory in the event of a loss of forced circulation. This paper describes the CATHENA model of the CANDU 9 shield cooling system and the simulation results of the loss of forced circulation event. In addition, this paper describes the results of a complete loss of flow in the end shield. These results show that the CANDU 9 end shield cooling system will continue to perform its function, thus ensuring lattice tube and fuel channel integrity under the postulated upset conditions.

1. INTRODUCTION

The CANDU 9 shield cooling system is designed to remove heat which accumulates in the reactor structures (shield tank and end shields) due to nuclear radiation from the reactor core and heat transferred from the fuel channels, heat transport system feeders, and moderator. This function of the shield cooling system is of particular importance in maintaining a stable temperature of the calandria and fueling tubesheets, thus ensuring lattice tube and fuel channel integrity. The other main function of this system is to maintain the shield tank and end shields full of water to provide biological shielding against radiation during normal operation and shutdown conditions.

The objective of this analysis is to show that the end shield cooling system is capable of providing sufficient thermosyphoning flow in the end shields in the event of loss of forced circulation, to remove the heat generated in the end shields with the reactor operating at 100% power. In addition, results are presented in this paper that show the behaviour of the end shield cooling system in the unlikely event of a complete loss of flow in the end shield, and in the event of loss of secondary flow to the heat exchanger in the shield cooling system.

2. ANALYSIS METHODOLOGY

2.1 The CATHENA Code

The analysis of the end shield cooling system was performed using the CATHENA thermalhydraulic code [1]. CATHENA is a one-dimensional, two-fluid thermalhydraulic code developed by AECL at Whiteshell Laboratories primarily for the analysis of postulated loss of coolant accident events in a CANDU reactor. The code has a general network capability and is capable of modelling the heat transfer phenomena occurring in CANDU type fuel channels and other components of the heat transport system. The code permits two dimensional (radial and circumferential) heat conduction modelling, and incorporates models for thermal radiation, Zr-steam reaction and solid-to-solid contact heat transfer. The heat transfer package is general and allows the connection of multiple wall surfaces to a single thermalhydraulic node. Extensive CATHENA validation has been completed involving various CANDU reactor components and

---

[1] MMIR Thermalhydraulics
[2] CANDU 9 Process
[3] CANDU 9 Process

transients, including validation of thermosyphoning in similar geometry to the CANDU heat transport system.

2.2 Description of the End Shield Cooling System

The shield cooling system is designed to facilitate enhanced thermosyphoning of the end shield inventory in the event of a loss of forced circulation [2,3]. A schematic diagram of the shield cooling system is shown in Figure 1. The end shield cooling flow is provided from the reserve water tank, located at a high elevation in the reactor building. Ion exchangers and filters are provided in the end shield cooling circuit for purification of the water in the circuit and the reserve water tank. The heat exchanger, which removes the heat from the shield cooling system, is also located at a high elevation, just below the reserve water tank. Any one of the two end shield pumps in the end shield circuit provides 100% forced circulation flow through the end shield (the other is in a standby mode). Also, one of the two shield tank pumps provides 100% forced circulation flow through the shield tank. The flow out of the end shield joins with the flow out of the shield tank, and is returned to the reserve water tank via the heat exchanger. Differences in water temperature, and hence water density, between the inlet and the return water columns provide the driving force for natural convective circulation in the end shield loop in the event of loss of end shield pumps.

The CANDU reactor end shield consists of a cylindrical space between the calandria and the fueling tubesheets. It contains the shielding balls, and the lattice tubes which penetrate the tubesheets. Figure 2 shows a schematic diagram of a CANDU 9 end shield. The end shield cooling flow enters the end shield at the bottom, and exits at the top. However, to reduce the consequences of a break in the end shield cooling system, the inlet piping in the end shield is located within the end shield. Eight inlet nozzles are attached at the end of eight inlet pipes passing through the end shield. Since the interior of the end shield does not contain any barriers, the flow is not restricted in vertical direction or in horizontal direction perpendicular to the reactor axis.

The nuclear heating of the shielding balls and the tubesheets is not uniform across the end shield, and the temperature of the lattice tubes varies across the end shield. This causes a complex flow distribution and heat transfer in the end shield.

2.3 Shield Tank Circuit Assumptions and Models

Since the analysis in this paper is focused on the end shield cooling circuit, the shield tank cooling circuit model is simplified by not modelling the shield tank cooling pumps. Instead, as shown in Figure 3, a flow boundary conditions is applied at the shield tank inlet. Also, the head tank attached to the shield tank to provide atmospheric boundary condition, as shown in Figure 1, is not modelled. The heat generation in the shield tank is modelled by a heat boundary condition (heat deposition directly into the coolant).

The heat exchanger is modelled using the CATHENA heat exchanger model. This model does not include the secondary side of the heat exchanger. Instead, it represents the secondary side by a "sink" temperature only.

The purification ion exchangers and filters are modelled by a single pipe component connected to the end shield pump suction and discharge side. A purification flow of about 45 kg/s is modelled by selecting appropriate flow resistance at the connections of the purification line to the end shield pump suction and discharge sides. So, when the end shield pumps are assumed lost, the purification flow is lost as well.

The two end shields, including inlet and outlet piping, are modelled as one (i.e., volume is conserved). The end shield cooling pump trip is modelled by reducing the pump speed from

1800 RPM to zero in 10 s. The loss of heat exchanger secondary side flow is modelled by reducing the heat exchanger area from the nominal value to zero in 10 s.

The torus shaped reserve water tank is modelled as a vertical pipe, with the total volume and height equal to those of the actual reserve water tank. Heat conductance in vertical direction in the reserve water tank is accounted for. The top of the reserve water tank is connected to a atmospheric boundary condition. No water level decrease was modelled in the reserve water tank in any of the postulated transients described in this paper. Also, no breaks in the shield tank system piping were included in this model.

2.4 End Shield Circuit Assumptions and Models

Two- or three-dimensional flow patterns are likely to develop in the end shields due to their complex geometry. Since CATHENA is a one-dimensional code, several assumptions are introduced in this analysis to facilitate the modelling.

Homogeneous distribution of the shielding balls is assumed in the end shield. The theoretical "rhombohedral" packing of the shielding balls yields about 25.9% porosity of the end shield space. However, to account for non-homogeneous effects, such as those created by the lattice tubes, the end shield porosity is assumed to be 40% in this model. The shielding balls are modelled as a number of vertical wall structures with the total area and volume equal to these of the actual shielding balls.

The lattice tubes are modelled as vertical wall structures and the assumed orientation of the end shield is in the vertical direction. The total surface area and volume of the lattice tube wall models is the same as those of the actual lattice tubes.

As shown in Figure 3, the end shield space is sub-divided into eight vertical flow paths, each modelled by a number of vertical pipe components, and each connected to an inlet and outlet pipe component. The flow area of each vertical flow path is equivalent to the flow area of the end shield encompassing three lattice tubes, except for the first and the last flow path that represent the sides of the end shield. No cross mixing is assumed between the vertical flow paths. Appropriate junction resistance is selected at each connection of an inlet pipe to a vertical flow path in the end shield model to adjust the flow. The results shown in this paper are obtained in simulations which assumed uniform distribution of the flow between the vertical flow paths.

Four types of wall models, attached to the vertical flow paths in the end shield, are used in this model to represent heat transfer from the calandria tubesheet, the fuelling tubesheet, the lattice tubes, and the shielding balls to the end shield coolant. No heat transfer between the wall models is taken into account in this model. The total surface area and the volume of all wall models used in this idealization of the end shield match the surface area and volume of the actual end shield wall structures. To achieve this, the number of wall models for the shielding balls and the lattice tubes are appropriately selected. One wall model is used for the calandria tubesheet and one wall model for the fuelling tubesheet. Therefore, the inner and outer radius of these wall models is appropriately adjusted to match the actual volume and surface area of the tubesheets. The heat transfer occurring between each of the above wall models and the end shield water is modelled using the CATHENA default heat transfer coefficients over the entire boiling curve.

A summary of heat deposition in all wall models described above is shown in Table 1 (both end shields combined). The reactor is assumed to operate at 100% power in all transients described in this paper. The heat deposition used in this analysis includes 30% contingency due to uncertainties in heat deposition rates. The heat deposition of 0.21 MW from all other sources is modelled as a heat boundary condition and is deposited directly into the end shield water. The heat transferred from/to the shield tank walls is neglected in the present model. Spatially variable heat generation from nuclear radiation is modelled in all wall structures in this model

Table 1: Heat Deposition in the CANDU 9 End Shield

PARAMETER	HEAT LOAD [1] (MW)
Nuclear heat deposited in shielding balls	0.22
Nuclear heat deposited in lattice tubes	0.082
Nuclear heat from other sources	0.21
Nuclear heat deposited in the calandria tubesheet	1.01
Heat transferred from the primary cooling system	4.68
Heat transferred from the fuelling tubesheet	0.45
Total heat deposited in the end shield	6.65
Heat deposited in the shield tank	2.61
Total heat deposited	9.26

[1] Both end shields combined

The model used in this analysis does not account for variation in outlet temperatures in different reactor channels. Instead, a constant inner temperature of 288°C is assumed in all lattice tubes, regardless of the location across the end shield. Also, a constant heat transfer coefficient of 57000 $W/m^2{}^\circ C$ at the inner side of the lattice tube wall is assumed. The properties of the gap between the end fitting and the lattice tubes are constant and tuned in this analysis (heat conductance of 42 $W/m^2{}^\circ C$ and emissivity of 0.25) to transfer 4.68 MW to the end shield water at normal design conditions (see Table 1).

The heat transfer from the calandria tubesheet to the moderator is assumed uniform across the tubesheet. The moderator temperature is assumed constant at 57°C, whereas the heat transfer coefficient at the interface between the tubesheet and the moderator is assumed at 12500 $W/m^2{}^\circ C$. This values are tuned to ensure that the total amount of heat transferred to the end shield water is about 1.01 MW during normal operation (see Table 1). Note that the total amount of heat deposited in the calandria tube sheet is 2.09 MW, but it is split and transferred to both sides of the tubesheet into the moderator and end shield water.

No heat generation is assumed in the fuelling tubesheet in this analysis. However, a certain amount of heat from the heat transport system is transferred from the end fittings and the feeders to the air in the space of the end shield enclosure. To account for this heat transfer, the air temperature at the outside of the fuelling tubesheet is specified at 288°C, and the heat transfer coefficient to the air at 38 $W/m^2{}^\circ C$. The selected air temperature and the heat transfer coefficient result in a volume average temperature of the fuelling tubesheet of about 75°C, and the net heat transfer to the end shield water of about 0.45 MW.

3. ANALYSIS OF RESULTS

The selection of scenarios simulated and described in this paper is based on the objectives of the analysis, i.e., to provide a best-estimate analysis of the loss of forced circulation event in the end shield, to examine the impact of the loss of secondary flow to the heat exchanger, and to estimate the consequences of the event of complete loss of flow in the end shield.

3.1 Loss of Forced Circulation in the End Shield

In the event of loss of forced circulation in the end shield circuit, natural circulation is expected to provide sufficient cooling with the reactor continuing to operate at 100% power. Figures 4 and 5 show the predicted mass flow rates and coolant temperatures during this transient assuming that the shield tank pumps keep operating. The simulation was run until 30000 s (about 8 hours) after the initiating event.

Figure 4 shows that the total end shield flow was predicted to decrease from about 100 kg/s (normal design flow) to about 10 kg/s when the end shield pumps were lost. With the resulting decrease in coolant velocity, the coolant transit time in the end shield increased, and therefore, the amount of heat transferred from the wall to the coolant also increased. All this resulted in an increase of coolant temperature (decrease in coolant density) at the outlet of the end shield. The corresponding decrease of coolant density at the outlet of the end shield provided good conditions for establishing natural circulation between the end shield and the heat exchanger and the reserve water tank located high above the end shield. This can be seen in Figure 4 as an increase in flow in the first 2500 s of the simulation after the pumps were lost. The end shield flow stabilised at about 26 kg/s.

Sensitivity simulations were performed by varying the water temperature and flow at the outlet of the shield tank to assess the impact on the thermosyphoning flow in the end shield circuit. As expected, when the flow was reduced from the shield tank, or the temperature was increased, higher thermosyphoning flow was predicted in the end shield circuit. When both the shield tank pumps and the end shield pumps were assumed lost at the same time, the predicted thermosyphoning flow in the end shield circuit was predicted to increase.

Figure 4 also shows the flow distribution between the flow paths in the end shield. Higher flow was predicted in the middle flow path than in the outside flow path. This is attributed to higher heat generation in the middle section of the end shield, i.e., higher water density difference.

Figure 5 shows the water temperature predicted at the top of the end shield. The water temperature increased in the period until 2500 s when the flow in the end shield decreased because the water was predicted to spend longer time in the end shield. After 2500 s, the water temperature stabilised, and a higher temperature by about 20°C was predicted in the middle than in the outer flow path (due to higher heat generation in the middle portion of the end shield).

A combined loss of forced circulation in the end shield circuit and the shield tank circuit was also simulated. The results were similar to the results in the case of loss of forced circulation in the end shield circuit.

3.2 Loss of Forced Circulation in the End Shield Circuit and Loss of Secondary Flow to the Heat Exchanger

Loss of secondary flow to the heat exchanger was analysed in combination with the loss of forced circulation in the end shield circuit to assess the effect of water heatup in the reserve water tank. Figure 6 shows the predicted fluid temperatures at the top of the end shield during this event. The predicted thermosyphoning flow (not shown in a figure) was not affected by the loss of the heat exchanger and was similar to the predicted flow in the event of loss of forced circulation in the end shield.

As evident from Figure 6, relatively rapid temperature increase of the coolant was predicted during the first 2500 s, as thermosyphoning developed. A slow temperature increase was predicted in the rest of the simulation, resulting from the heat deposition in the reserve water tank, and corresponding increase of the water temperature at the inlet of the end shield. However, the water temperature at the top of the end shield was still subcooled 8 hours after the initiating event.

3.3 Complete Loss of Flow in the End Shield

No pipe break in the CANDU 9 end shield cooling system can cause draining of the end shield water because the end shield inlet piping enters from the top and extends to the bottom of the end shield. Therefore, the end shield will remain filled with water no matter where the break is postulated in the end shield circuit. In an unlikely event of a break in the inlet or outlet pipe above the end shield, the water inventory above the end shields would be discharged through the break in about 20 minutes. Following the loss of this water inventory, the end shield will remain filled with stagnant water, which will heat up and boil off, thus gradually uncovering the tubesheets. This transient was simulated with CATHENA to assess the tubesheet temperature increase. At the beginning of the transient, it was assumed that the water inventory above the end shields is lost, and complete flow stagnation is established in the end shield.

Figure 7 shows the predicted void fraction at the bottom of the end shield. About 3500 s after the initiating event, the water temperature at the bottom of the end shield reached the saturation temperature, and the void fraction was predicted to increase, i.e., boiling to start. By about 14000 s after the initiating event, the water level reached the bottom of the end shield, i.e., a complete dryout of the end shield was predicted.

Figure 8 shows the predicted wall average temperatures at three elevations of the end shield (top, middle and bottom). The predicted initial temperature rise in the first 2500 s is associated with the heatup of the end shield water to saturation (from 100°C to 125°C, depending on the elevation). At the top of the end shield, the wall average temperature continued to increase after reaching saturation because the top of the end shield was first uncovered. At the bottom, since it was uncovered last, the wall average temperature stagnated until about 14000 s, and then started to increase gradually after the wall was uncovered. The calandria tubesheet average wall temperature was not predicted to increase after the wall was uncovered because the outer side of the calandria tubesheet was in contact with the moderator at relatively low temperature at all times, and therefore good cooling was provided. The lattice tube average wall temperature remaned constant after reaching the temperature of the primary coolant (288°C). A continuous and significant increase of the average wall temperature of the fuelling tubesheet and the shielding balls was predicted after uncovering and throughout the transient due to lack of cooling.

4. SUMMARY AND CONCLUSIONS

A CATHENA model of the CANDU 9 shield cooling system was developed and used to simulate selected abnormal events involving loss of forced circulation and loss of flow in the end shield circuit. The simulations were conducted for 8 hours of real time, to assess the consequences of these events during an 8-hour operator shift. It was postulated that in all simulated transients the reactor would continue to operate at 100% power, and that the reactor operator would not undertake any mitigating actions. The results of the analysis show that the CANDU 9 end shield cooling system will continue to perform its function, thus ensuring lattice tube and fuel channel integrity under the postulated upset conditions.

In the event of loss of forced circulation in the shield cooling system, the results of this analysis have shown that the CANDU 9 shield cooling system is capable of developing thermosyphoning flow of about 26 kg/s, which is sufficient to provide effective cooling of the end shield with the reactor operating at 100% power.

REFERENCES

1. B.N. Hanna, "CATHENA: A Thermalhydraulic Code for CANDU Analysis," Nuclear Engineering and Design, NED-97-549, Accepted for Publication, 1997.
2. K.R. Hedges, S.K.W. Yu, J.M. Hopwood, J.M. Cuttler, "Advances in PHWR Design," 5th International Meeting on Nuclear Thermal Hydraulics, Operations & Safety (NUTHOS-5), Beijing, China, April 13-16, 1997.
3. V.G. Snell, N.J. Spinks, CANDU Safety: Evolution and Recent Advances," 5th International Meeting on Nuclear Thermal Hydraulics, Operations & Safety (NUTHOS-5), Beijing, China, April 13-16, 1997.

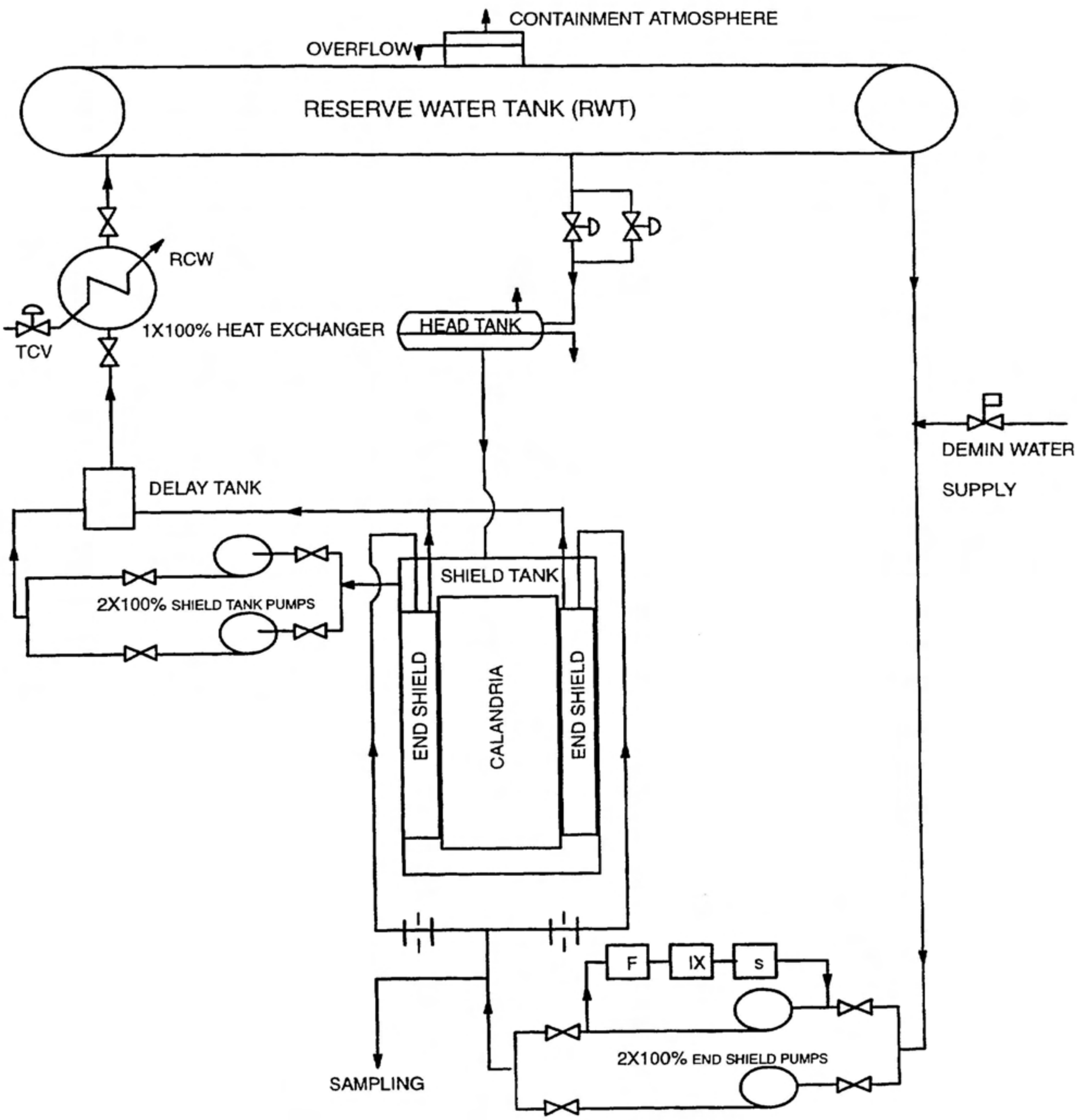

Figure 1: Schematic Diagram of the CANDU 9 Shield Cooling System

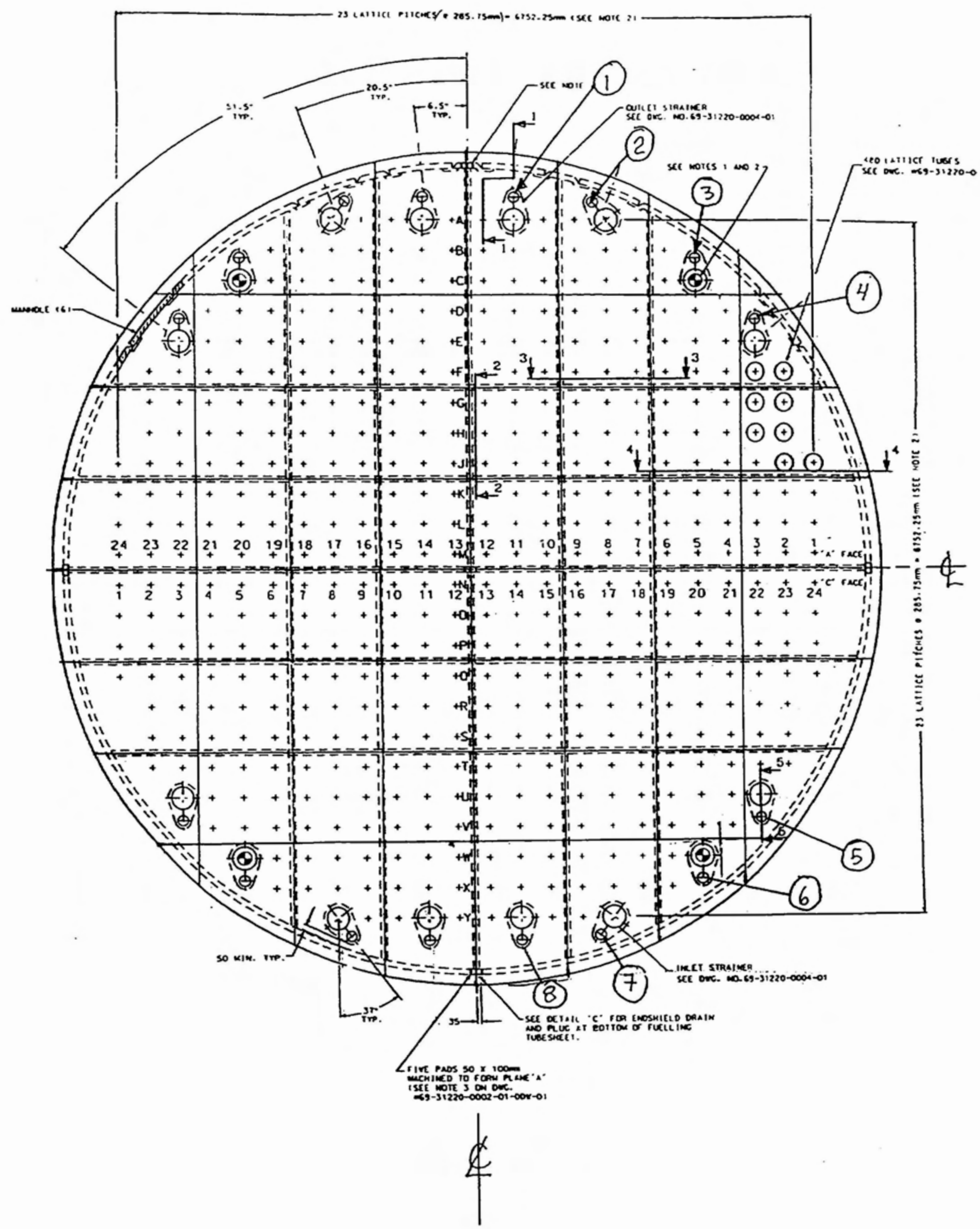

Figure 2: Schematic Diagram of the CANDU 9 End Shield

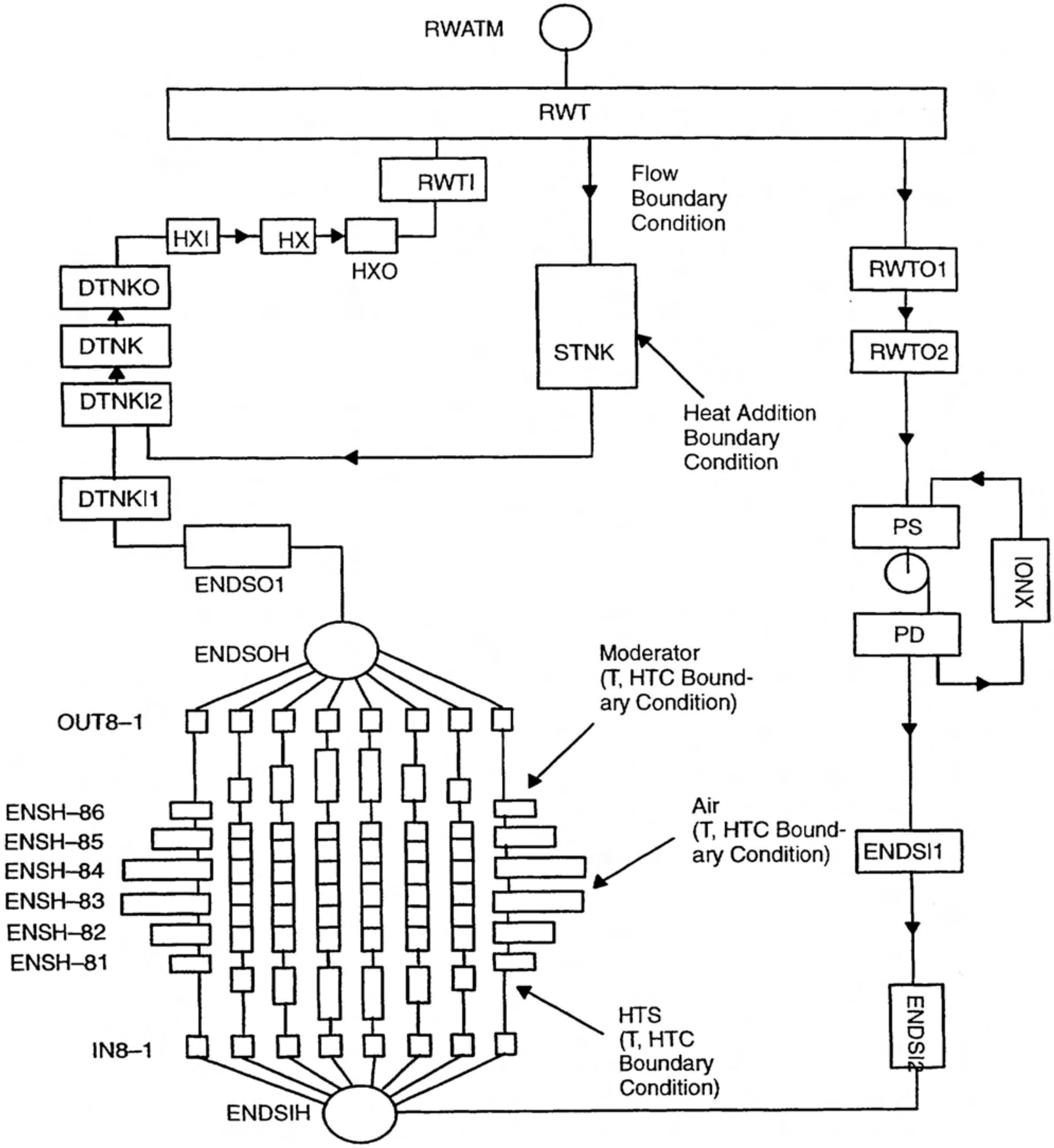

Figure 3: CATHENA Model of the CANDU 9 Shield Cooling System

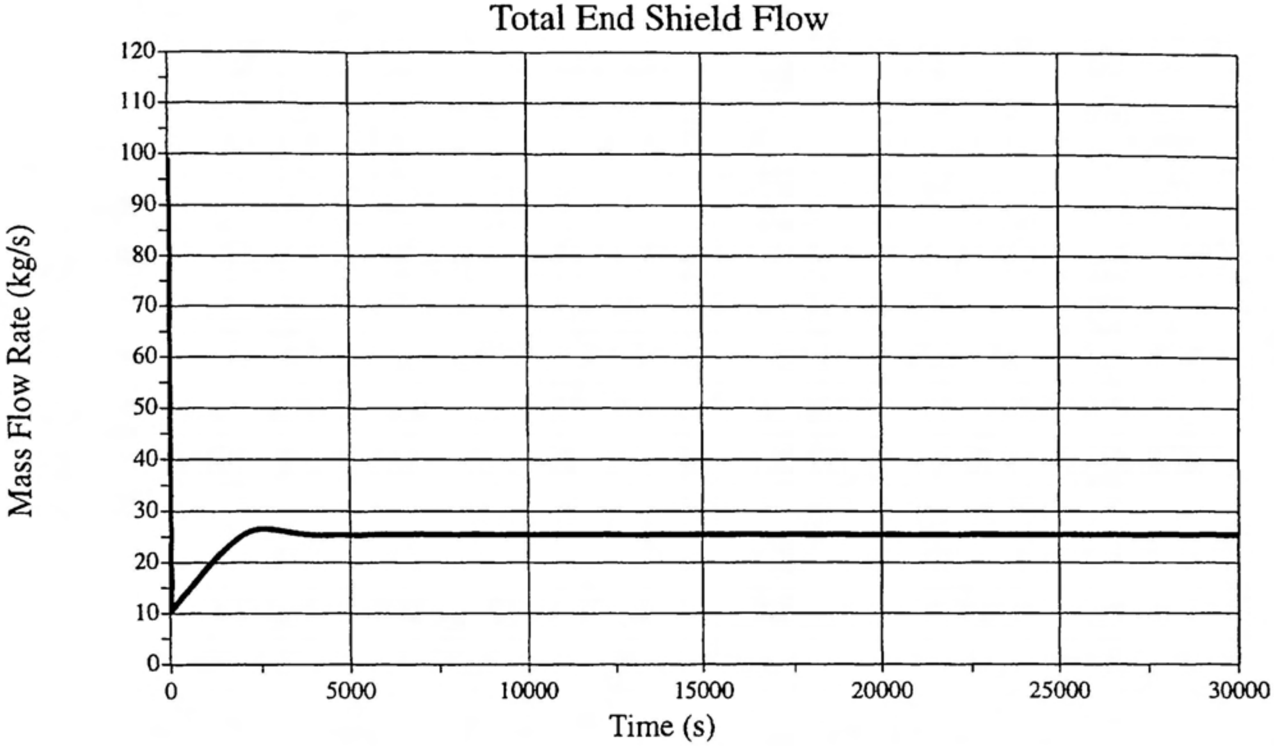

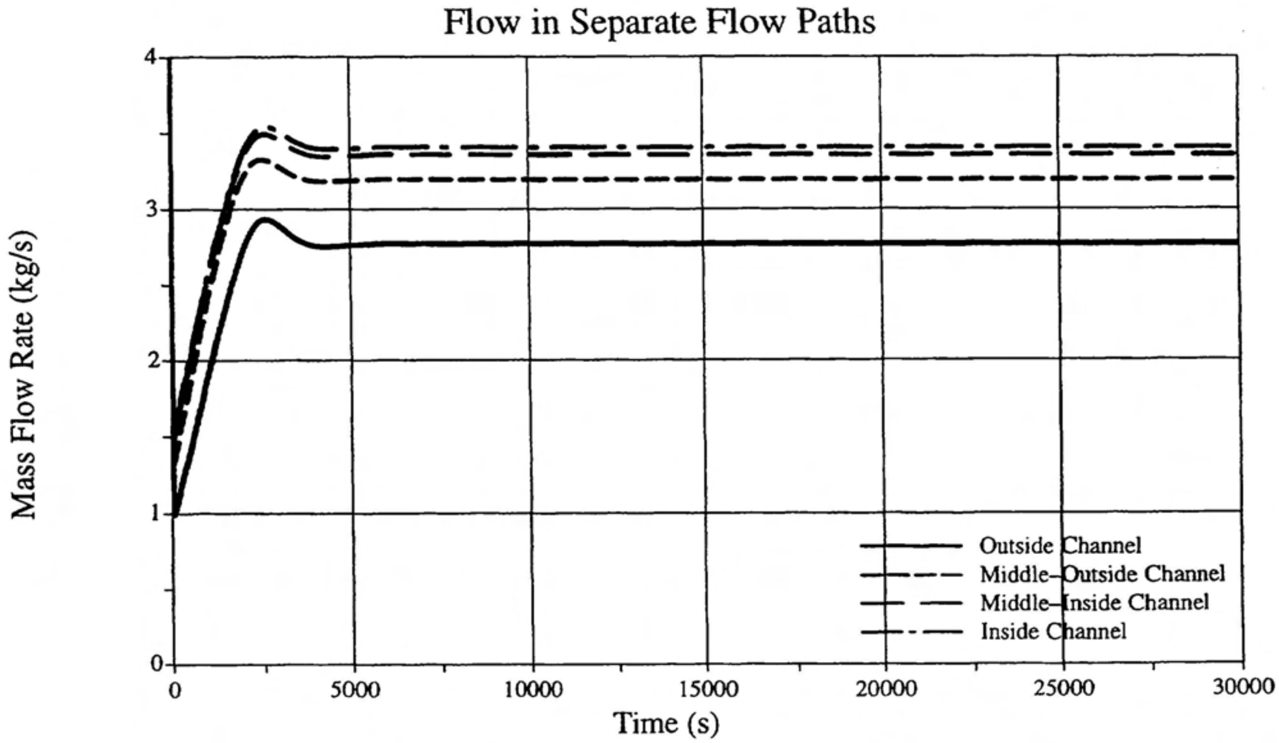

Figure 4: Predicted Mass Flow Rates in the Event of Loss of Forced Circulation

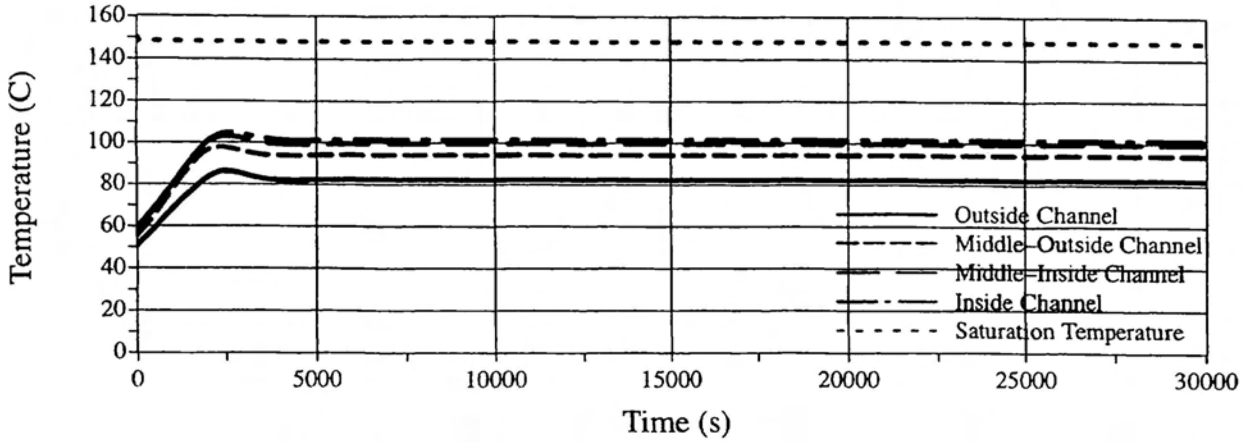

Figure 5: Predicted Coolant Temperatures at the Top of the End Shield in the Event of Loss of Forced Circulation

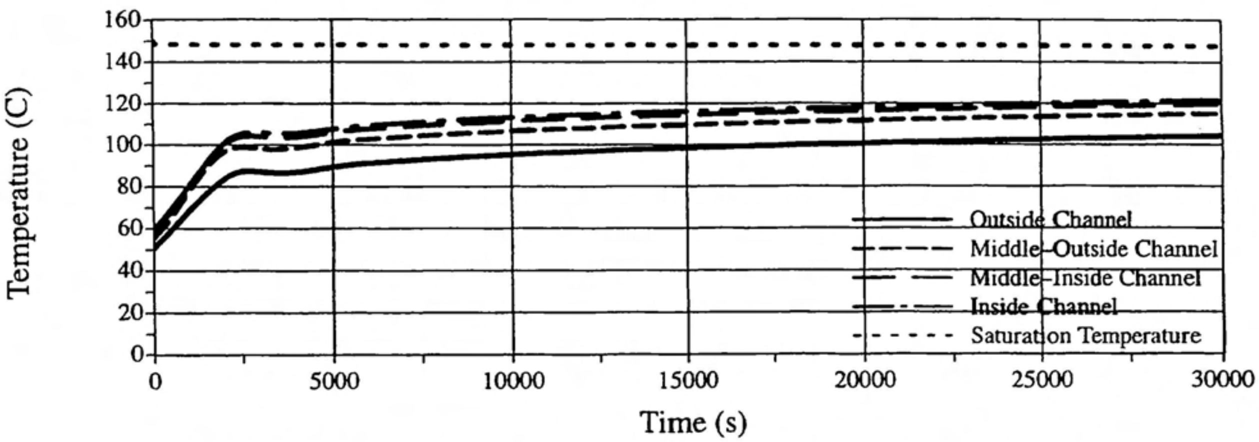

Figure 6: Predicted Coolant Temperatures at the Top of the End Shield in the Event of Loss of Secondary Flow to the Heat Exchanger

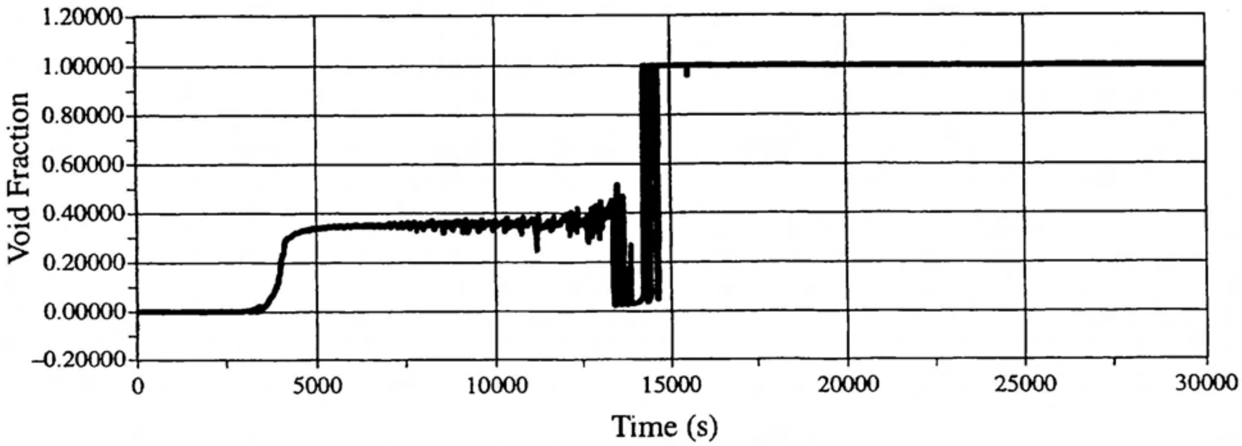

Figure 7: Predicted Void Fraction in the End Shield in the Event of Complete Loss of Flow

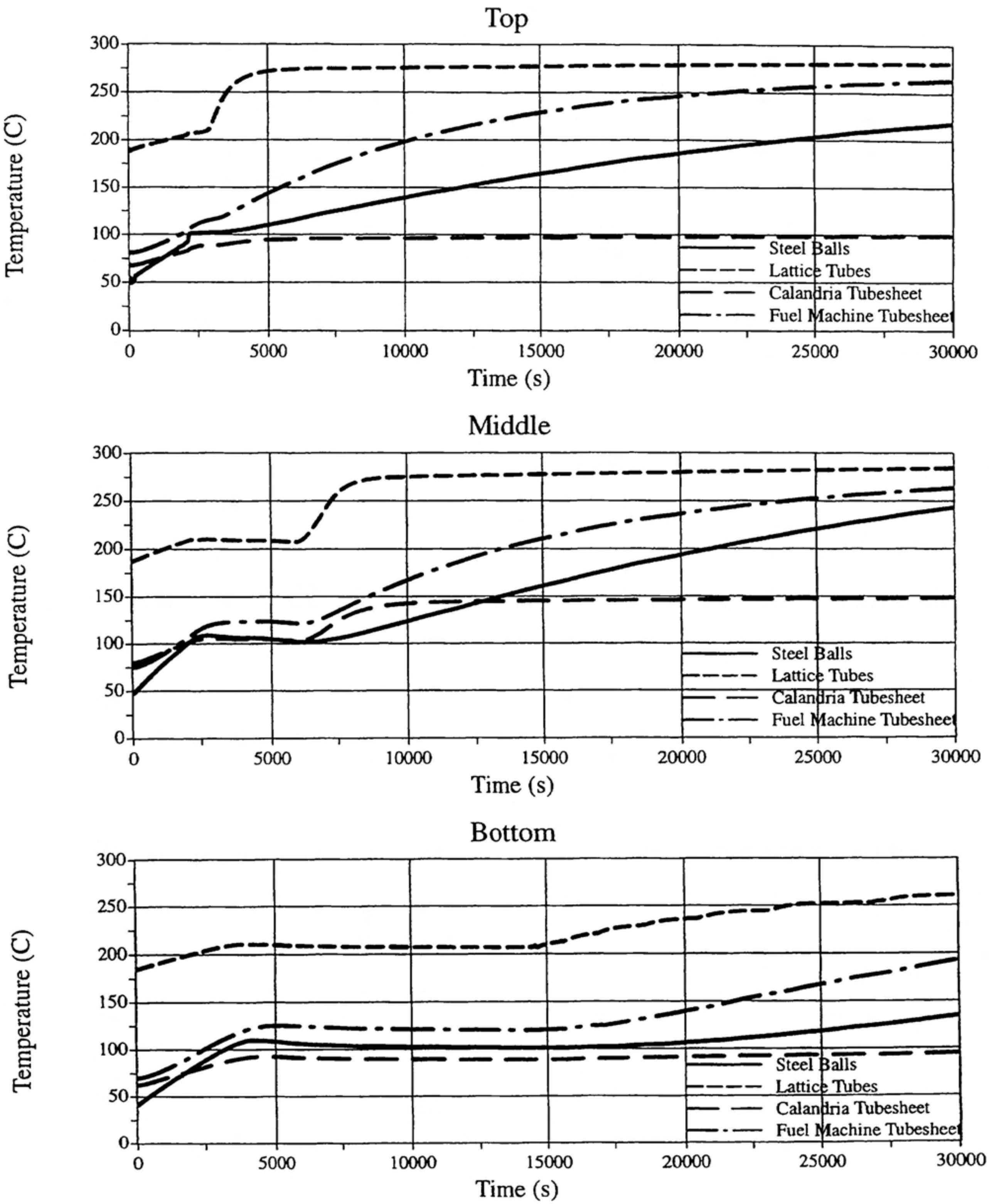

Figure 8: Predicted End Shield Wall Temperatures in the Event of Complete Loss of Flow